FUEL/CLADDING COMPATIBILITY IN IRRADIATED METALLIC FUEL PINS AT ELEVATED TEMPERATURES*

by

Hanchung Tsai

Materials and Components Technology Division
Argonne National Laboratory
Argonne, Illinois 60439-4838

CONF-900804--9

DE90 010129

April 1990

DISCLAIMER

Paper to be published in the Proceedings of the 1990 International Fast Reactor Safety Meeting, sponsored by the American Nuclear Society, August 12-16, 1990, Snowbird, Utah.
*Work supported by the U.S. Department of Energy, Office of Technology Support Programs, under Contract W-31-109-Eng-38.

FUEL-CLADDING COMPATIBILITY IN IRRADIATED METALLIC FUEL PINS AT ELEVATED TEMPERATURES

Hanchung Tsai

Argonne National Laboratory
Argonne, Illinois 60439, U.S.A.

ABSTRACT

Over fifty fuel/cladding compatibility tests on irradiated metallic fuel specimens have been conducted in an in-cell facility at elevated temperatures. At temperatures below 700-725°C, no fuel/ cladding interaction was noted in tests up to 7 h. Liquid-phase cladding penetration occurred in some of the tests at temperatures greater than 725-750°C. The effective rates of liquid-phase cladding penetration of six different fuel/cladding combinations during 1-h testing are reported. After the initial liquefaction at the fuel/ cladding interface, which may be affected by the solid-state diffusional interaction during the steady-state irradiation, the rate of further cladding penetration stays constant or decreases with time. There was no runaway cladding penetration in the latter part of a heating cycle.

INTRODUCTION

The principal advantages of the Integral Fast Reactor (IFR), an advanced liquid-metal-cooled fast reactor, include improved reactor safety, fuel cycle economics, and environment protection.[1,2] These advantages are the direct results of the employment of a metallic alloy, containing U, Pu, and Zr, as the driver fuel material.

The U and Pu constituents in the metallic fuel, and the rare earth fission products generated during the irradiation, however, have a propensity of interacting metallurgically with the stainless steel cladding at elevated temperatures.[3,4] During the steady-state irradiation, solid-state interdiffusion across the fuel/cladding interface may occur. If the fuel pin is then subjected to a high temperature off-normal reactor event, the interdiffusion layers on the fuel and cladding inside surface may liquefy, dissolving additional fuel, and causing liquid-phase penetration into the cladding. To assess the effects of such interactions on the reliable performance of the IFR fuel pins under off-normal reactor conditions, it is necessary to determine (1) the temperature above which liquid-phase cladding penetration would occur and (2) the rate of such penetration into the cladding.

This paper summarizes the on-going experimental effort in studying the compatibility between the irradiated metallic fuel and cladding at elevated temperatures. An underlying objective of the work has been to support the development of driver fuel types for the Experimental Breeder Reactor-II (EBR-II) and the advanced liquid metal reactor, PRISM.[5] Currently, the driver fuels for EBR-II are U-10 w/o Zr binary alloy clad in either 316, D9 or HT9 stainless steels. That for the PRISM reactor is a U-26 w/o Pu-10 w/o Zr fuel clad in HT9 steel.

EXPERIMENTAL

All of the data presented in this paper were generated in an in-cell facility, called the fuel behavior test apparatus (FBTA), located in the Alpha-Gamma Hot Cell (AGHC) at the Argonne National Laboratory. The specimens used in the tests were obtained from fuel pins irradiated under steady-state conditions in EBR-II.

A quad-elliptical radiant furnace powered by four longitudinal infrared filaments provides the isothermal heating of the specimen. The test specimen is usually a short section of an irradiated fuel pin placed inside a slightly taller cup. Shaped and highly reflective surfaces behind the filaments focus the radiant energy onto the centerline of the furnace where the specimen/cup is located. A single bare-wire Pt/Pt-Rh thermocouple welded onto the outside of the specimen cup monitors the specimen temperature. The output from the thermocouple is used to control the furnace, by way of a microcomputer and a feedback algorithm, to maintain the desired test temperature. Owing to the negligible thermal inertia of the infrared filaments and the strong focusing of the radiant energy, heat-up of the specimen to the desired test temperature typically takes less than 1 min. As heat is externally provided to the specimen, once the desired test temperature is reached, no significant radial temperature gradient exists in the fuel or the cladding.

During the experiment, the specimen is shielded from the hot cell environment by two concentric quartz tubes. A high purity helium purge flow in the inner quartz tube provides an inert atmosphere for the test specimen. The fission gas released from the open ends of the fuel specimen during the test is carried away by the helium purge gas to an ex-cell ionization chamber for monitoring the ^{85}Kr activity. If required, the released gas can be collected with a liquid-nitrogen-cooled charcoal trap for later quantitative analysis. A linear-variable-displacement transducer, attached to the top end of the hold-down rod resting on top of the test specimen is used to measure fuel expansion or contraction during the test. A more detailed description of the FBTA can be found in Ref. 6.

Following the test, metallographic examination of the specimen using one of the two shielded metallographs in the AGHC is conducted to collect the evidence of fuel/cladding interaction and to determine the maximum depth of cladding penetration. From these data, the liquid-

phase formation temperature and the maximum cladding penetration rates are derived. Selected specimens are further examined with the shielded electron microprobe and scanning electron microscope in the AGHC facility to delineate the constituent distribution in phases formed in the fuel/cladding interaction zone.

TEST RESULTS AND DISCUSSION

Over fifty test on U-26Pu-10Zr/316SS, U-19Pu-10Zr/HT9, U-19Pu-10Zr/D9, U-10Zr/HT9, U-10Zr/D9 and U-10Zr/316SS specimens have been conducted. The burnups of the fuel were between 3 to 17 a/o. All tests are of the constant-temperature type; the temperature and duration of the tests ranged from 700 to 850°C and 0.1 to 7.0 h, respectively. The matrix of the tests conducted is given in Table I.

Types of Fuel/Cladding Interaction

At temperatures below ~700-725°C, no liquid-phase fuel/cladding interaction has been observed in the FBTA tests (with durations up to 7.0 h). In the temperature range of ~725-750°C, solid-state diffusional interaction occasionally can be noted, mostly in low burnup fuel with austenitic stainless steel cladding (Type 316 and D9). The reaction results in an austenitic-to-ferritic transformation due to the loss of Ni to the fuel. The diffusion of Cr and Fe away from the cladding matrix is not as noticeable. The diffusion of fuel components, including fission products, into the cladding also appears to be relatively slow. A section of the Type 316 stainless steel cladding that incurred diffusional reaction after the 88-27 test (740°C for 7.0 h) is shown in Fig. 1. Data from hardness measurements showed no significant loss of ductility of the affected cladding.

At temperatures ~725°C and above, the interaction between the fuel and cladding may result in liquid-phases cladding penetration. Two types of interaction, e.g., grain boundary penetration and matrix dissolution, have been found. Liquid-phase grain boundary penetration occurs predominantly in high burnup fuel. Figure 2 shows a section of the D9 cladding from the 90-01 test affected by grain boundary interaction. The liquid phase on the cladding grain boundary consists mainly of the fission product lanthanides, e.g., La, Pr, Nd, and Ce. The content of fuel constituents U and Pu in the liquid phase was minor. The cladding grains surrounded by the liquid phase appear to undergo an austenitic-to-ferritic transformation. Diffusion of Fe into the fuel matrix appears to be minor. There are currently no FBTA test data on high burnup fuels clad with HT9 cladding.

Table I

FBTA Compatibility Test Matrix

Test No.	Fuel/Cladding	Pin No.	EBR-II S/A	Peak BU (a/o)	Axial Loc. x/L	Test Temp. (C)	Test Time (Hr)
87-74	U-19Pu-10Zr/HT9	T459	X425	3	0.69	700	1.0
87-75	U-19Pu-10Zr/HT9	T459	X425	3	0.71	750	1.0
87-76	U-19Pu-10Zr/HT9	T459	X425	3	0.74	780	1.0
88-01	U-10Zr/HT9	T437	X425	3	0.85	800	1.0
88-02	U-10Zr/HT9	T437	X425	3	0.87	850	1.0
88-03	U-10Zr/HT9	T437	X425	3	0.89	750	1.0
88-04	U-10Zr/HT9	T437	X425	3	0.46	800	1.0
88-05	U-10Zr/HT9	T437	X425	3	0.48	750	1.0
88-06	U-10Zr/HT9	T437	X425	3	0.52	700	1.0
88-13	U-10Zr/HT9	T437	X425	3	0.56	725	1.0
88-07	U-10Zr/D9	T224	X420	6	0.93	800	1.0
88-08	U-10Zr/D9	T224	X420	6	0.91	750	1.0
88-09	U-10Zr/D9	T224	X420	6	0.89	725	1.0
88-11	U-10Zr/D9	T248	X421	10	0.76	750	1.0
88-12	U-10Zr/D9	T248	X421	10	0.78	800	1.0
88-14	U-10Zr/D9	T248	X421	10	0.74	800	1.0
88-15	U-10Zr/HT9	T619	X429	8	0.46	800	1.0
88-16	U-10Zr/HT9	T619	X429	8	0.55	800	0.5
88-17	U-10Zr/HT9	T619	X429	8	0.23	800	2.0
88-18	U-10Zr/HT9	T619	X429	8	0.20	800	1.0
88-19	U-10Zr/HT9	T619	X429	8	0.25	800	0.5
88-20	U-10Zr/HT9	T619	X429	8	0.27	800	0.13
88-21	U-10Zr/HT9	T619	X429	8	0.30	800	0.25
88-22	U-26Pu-10Zr/316	T326	X423	5	0.54	700	1.0
88-23	U-26Pu-10Zr/316	T326	X423	5	0.60	750	1.0
88-24	U-26Pu-10Zr/316	T326	X423	5	0.57	800	1.0
88-25	U-26Pu-10Zr/316	T326	X423	5	0.45	670	7.0
88-26	U-26Pu-10Zr/316	T326	X423	5	0.63	850	1.0
88-27	U-26Pu-10Zr/316	T326	X423	5	0.48	740	7.0
88-28	U-26Pu-10Zr/316	T326	X423	5	0.40	710	7.0
89-01	U-26Pu-10Zr/316	T326	X423	5	0.42	770	7.0
89-02	U-10Zr/316SS	T536	X421	9	0.48	800	1.0
89-03	U-10Zr/316SS	T536	X421	9	0.52	850	1.0
89-04	U-10Zr/316SS	T536	X421	9	0.45	750	1.0
89-05	U-10Zr/316SS	T323	X423	5	0.55	800	1.0
89-06	U-10Zr/316SS	T323	X423	5	0.52	750	1.0
89-08	U-10Zr/316SS	T323	X423	5	0.45	850	1.0
89-13	U-10Zr/316SS	T323	X423	5	0.58	800	0.4
89-14	U-10Zr/316SS	T323	X423	5	0.61	800	0.2
89-15	U-10Zr/316SS	T323	X423	5	0.64	800	2.0
89-16	U-10Zr/316SS	T323	X423	5	0.67	800	4.0
89-09	U-26Pu-10Zr/316	T326	X423	5	0.70	800	1.0
89-10	U-26Pu-10Zr/316	T326	X423	5	0.73	800	2.0
89-11	U-26Pu-10Zr/316	T326	X423	5	0.78	800	4.0
89-12	U-26Pu-10Zr/316	T326	X423	5	0.80	800	0.4
90-01	U-19Pu-10Zr/D9	T106	X421	17	0.50	750	1.0
90-02	U-19Pu-10Zr/D9	T106	X421	17	0.87	750	1.0
90-03	U-19Pu-10Zr/D9	T106	X421	17	0.84	800	1.0
90-04	U-10Zr/D9	T227	X421	17	0.51	800	1.0
90-05	U-10Zr/D9	T227	X421	17	0.87	800	1.0
90-06	U-10Zr/D9	T227	X421	17	0.53	800	1.0
90-07	U-10Zr/D9	T227	X421	17	0.82	750	1.0
90-08	U-10Zr/D9	T227	X421	17	0.78	725	1.0
90-09	U-10Zr/D9	T227	X421	17	0.75	800	0.5
90-10	U-10Zr/D9	T227	X421	17	0.73	725	7.0

Fig. 1. Diffusional interaction in Type 316 stainless steel cladding. (1) intact cladding; (2) affected cladding; (3) Zr-rich surface layer on fuel from fabrication; (4) etched fuel. (Etched, 525X, MCT 246898)

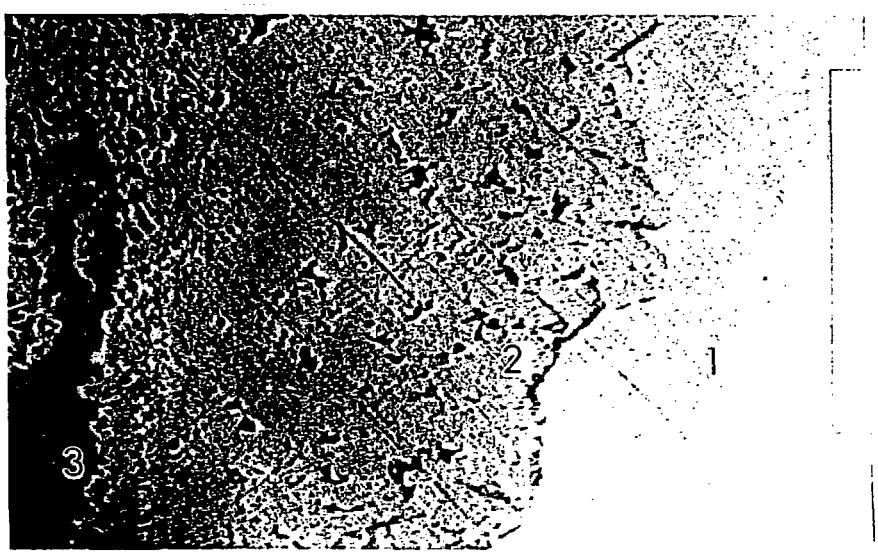

Fig. 2. Liquid-phase grain boundary penetration in D9 cladding from Test 90-01. (1) intact cladding; (2) reacted cladding; (3) lanthanide fission products. (As-polished, 500X, MCT 276570)

In lower burnup specimen, cladding penetration in the form of matrix dissolution prevails. The dissolved cladding components, mainly Fe (and Ni, in the case of austenitic cladding steel), react with the fuel and cause fuel liquefaction. Figure 3 shows the transverse section of the U-10Zr/HT9 specimen after the 800°C, 1.0-h, 88-04 test. A section of the reacted cladding under as-polished condition is shown in Fig. 4. The reacted cladding is brittle at room temperature and fractures readily. Figure 5 shows the backscattered electron image of the reacted cladding under the SEM and the compositions of the major phases in the reacted zone determined by energy-dispersive X-ray analyses. The composition of the unreacted cladding, both immediately adjacent to the well-defined reaction boundary and further away, was essentially that of the original HT9 material. No diffusional-controlled sub-phases or intergranular penetration ahead of the visible reaction boundary could be detected on the cladding side of the boundary at magnifications up to ~3000X.

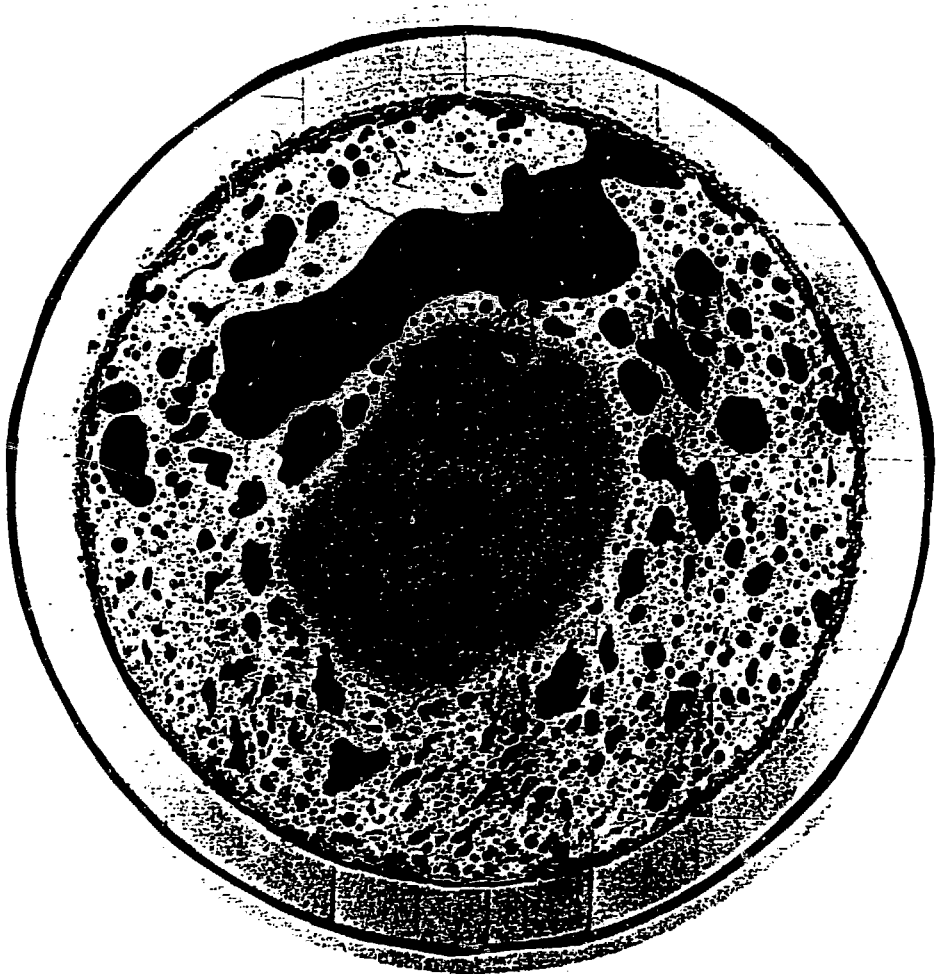

Fig. 3. Transverse section of the U-10Zr-HT9 specimen after the 88-04 test (800°C 1.0 h). Note fuel liquefaction except the center. (As polished, MCT 244038)

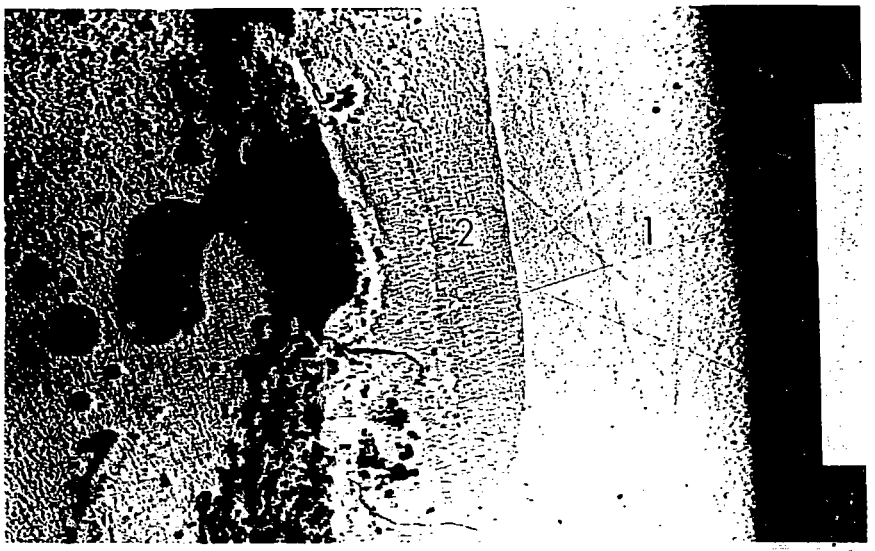

Fig. 4. Liquid-phase matrix penetration in HT9 cladding. (1) Intact cladding; (2) reacted cladding. (AP, 250X, MCT 244014)

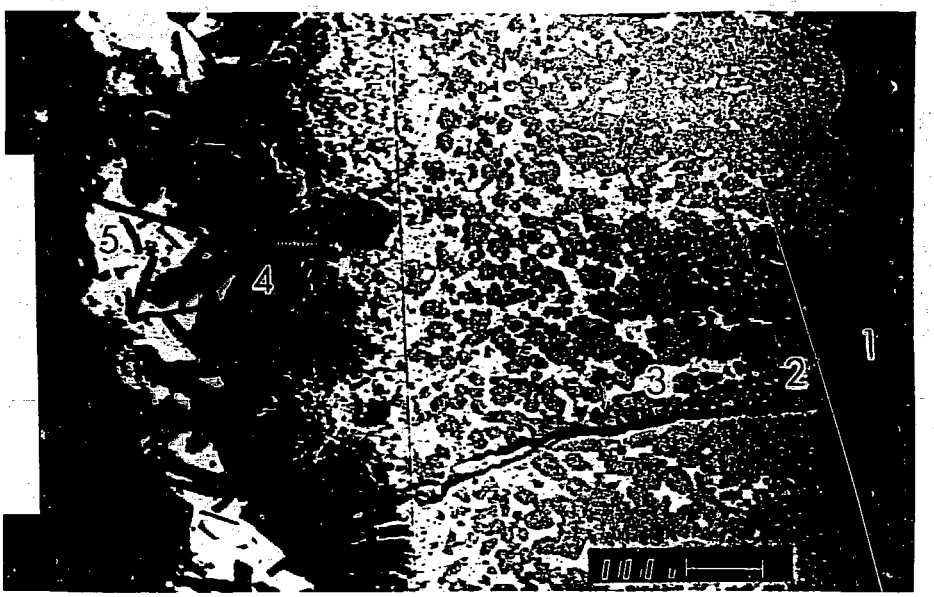

Fig. 5. Backscattered electron image of the cladding reaction zone in a U-10Zr/HT9 specimen. (1) Intact cladding; (2) dendritic phase; (3) matrix phase; (4) dark gray phase; (5) once-molten fuel.

	Composition (a/o)			
	U	Zr	Fe	Cr
1	–	–	88	12
2	16	3	70	11
3	67	3	28	2
4	2	32	49	17
5	67	5	28	–

Time-dependent Cladding Penetration Rate

A number of tests were performed on comparable specimens at the same temperature (800°C) but with different durations. The principal purpose of these test was to determine whether the penetration rate could vary precipitously with time, particularly at the latter part of a heating cycle. The results, summarized in Fig. 6, show that, after the initial rapid reaction, the penetration rate either remains constant or decreases with time. There is apparently no runaway penetration at any time during the tests. The rapid penetration at the onset of the heating is probably related to the fuel/cladding diffusional interaction occurring during the steady-state irradiation. The interdiffusion layers on the fuel and cladding surfaces, upon reaching the 800°C test temperature, apparently liquefied with little delay. After these layers are consumed, further penetration into the cladding is then controlled by the diffusion across the liquid/solid boundaries.

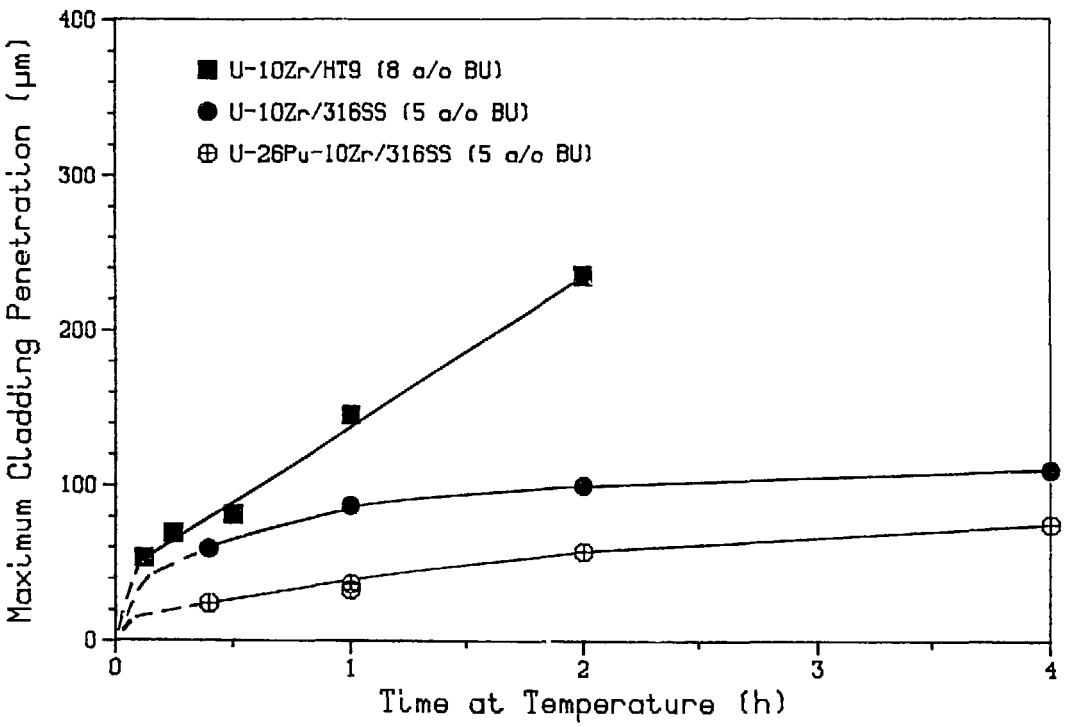

Fig. 6. Time-dependent cladding penetration at 800°C.

Temperature-Dependent Cladding Penetration Rate

A majority of the FBTA tests had a duration of 1.0 h. The rate of liquid-phase cladding penetration determined from these 1.0-h tests are shown in Fig. 7. (The penetration rate is defined as the measured maximum penetration divided by the 1 h test duration. It represents an effective rate and includes the accelerated penetration at the onset of heating). The data scatter in the liquefaction band shown in the figure is due mainly to the wide range of variables on material, irradiation conditions, and burnup. All of the test data, except one, can be enveloped by an empirical Arrhenius correlation

$$S = \exp[A-Q/RT].$$

where S = rate of liquid-phase penetration, in μ/s,
A = constant, 11.65,
Q = activation energy, -31.13 kcal/mole,
R = gas constant, 1.987 cal/mole K, and
T = temperature, K.

The exception is test 90-01 on a specimen from the midplane section of a high burnup (17 a/o) U-19Pu-10Zr/D9 pin. Because of the excessive cladding swelling (~7% diametral strain) near the midplane of this pin, a gap developed between the fuel and cladding during the steady-state irradiation. The extensive restructuring of the high Pu-content fuel during the irradiation due to the increased porosity resulted in an abnormally high accumulation of lanthanide fission products in the gap (see Fig. 2). The lanthanide ingots in the gap is apparently responsible for the enhanced cladding penetration. An identical test, 90-02, on a specimen obtained from the upper portion of the same pin where the cladding swelling was more modest (~1% strain), yielded a penetration rate only about one-fourth of that in the 90-01 test.

CONCLUSIONS

Three types of fuel/cladding interaction were identified in the compatibility tests conducted in the FBTA. There was no noticeable interaction at temperatures below 700-725°C. At higher temperatures, solid-state interdiffusion, liquid-phase grain boundary penetration, and liquid-phase matrix penetration have been found.

The temperature-dependent liquid-phase penetration follow an Arrhenius correlation. An enveloping penetration rate equation, developed from the 1-hr test data, may be used to evaluate fuel-pin cladding wastage during an off-normal reactor event having a comparable duration.

The presence of lanthanide fission products in the fuel/cladding gap was found to have a significant impact on the cladding penetration rate in austenitic stainless steel claddings. The effects of fission products on non-swelling, tempered martensitic steel cladding HT9 remain to be investigated.

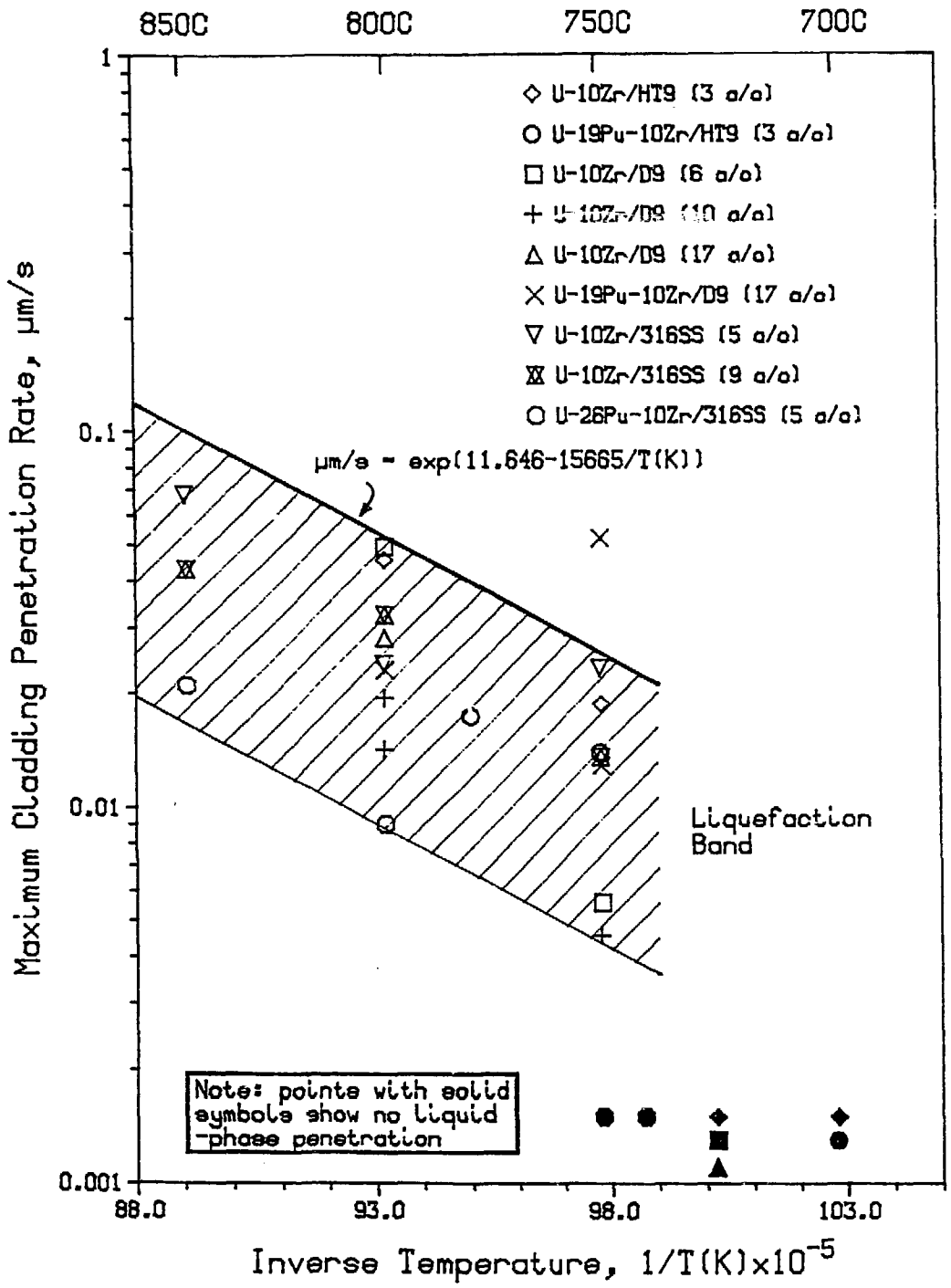

Fig. 7. Effective cladding penetration rates for specimens tested for one hour.

ACKNOWLEDGMENTS

This work was performed under the auspices of the U. S. Department of Energy. The author wishes to thank L. A. Neimark for many valuable and helpful discussions.

REFERENCES

1. J. F. MARCHATERRE et al., "Integral Fast Reactor Concept Inherent Safety Features," ASME Winter Meeting, 86-WA/NE-14, Anaheim, CA., 1986.

2. Y. I. CHANG, "The Integral Fast Reactor," Nucl. Tech., 88, 129 (November 1989).

3. S. T. ZEGLER and C. M. WALTER, "Compatibility Between U-Pu-based Fuels and Potential Cladding Materials," AIME Nuclear Metallurgy Symposium on Plutonium Fuels Technology, AIME 13, October 1967.

4. G. L. HOFMAN et al., "Chemical Interaction of Metallic Fuel With Austenitic and Ferritic Stainless Steel Cladding," International Conference on Reliable Fuels For Liquid Metal Reactors, Tucson, Az., 1986.

5. PRISM

6. HANCHUNG TSAI, "A Versatile Apparatus For Studying The Behavior of Irradiated Fuel," to be published in the ANS 37th Remote Systems Technology Division Proceedings, San Francisco, CA., November 1989.